

RESEARCH ARTICLE

MATERIALS SCIENCE

Autonomous alignment and healing in multilayer soft electronics using immiscible dynamic polymers

Christopher B. Cooper^{1†}, Samuel E. Root^{1†}, Lukas Michalek¹, Shuai Wu², Jian-Cheng Lai¹, Muhammad Khatib¹, Solomon T. Oyakhire¹, Renee Zhao², Jian Qin¹, Zhenan Bao^{1*}

Self-healing soft electronic and robotic devices can, like human skin, recover autonomously from damage. While current devices use a single type of dynamic polymer for all functional layers to ensure strong interlayer adhesion, this approach requires manual layer alignment. In this study, we used two dynamic polymers, which have immiscible backbones but identical dynamic bonds, to maintain interlayer adhesion while enabling autonomous realignment during healing. These dynamic polymers exhibit a weakly interpenetrating and adhesive interface, whose width is tunable. When multilayered polymer films are misaligned after damage, these structures autonomously realign during healing to minimize interfacial free energy. We fabricated devices with conductive, dielectric, and magnetic particles that functionally heal after damage, enabling thin-film pressure sensors, magnetically assembled soft robots, and underwater circuit assembly.

Self-healing allows soft electronic devices to recover from various forms of damage, such as punctures, scratches, and slices, to improve device robustness and lifetime. Previous work has demonstrated self-healing polymers that use a range of dynamic bonds, such as hydrogen bonding (1–3), metal-ligand coordination (4–6), or dynamic covalent bonds (7). These polymers are generally insulating, thus, to make functional electronic devices, they are embedded with conductive or dielectric materials (e.g., particles, nanowires, nanotubes, flakes, etc.) to achieve the desired bulk electrical properties while retaining the soft mechanical properties of the self-healing polymer matrix. These self-healing composites can recover not only their original mechanical properties upon healing but also their electrical conductivity (8).

Many self-healing devices have been reported, including aquatic skin, field-effect transistors, light-emitting capacitors, battery-based sensors, and advanced multifunctional sensing platforms (9–11). As the complexity of devices has increased, it has become necessary for self-healing to simultaneously occur between multiple layers with different functions. This concept was shown for an electronic skin that integrated multiple functional components, but thick layers and careful manual alignment were needed to ensure functional self-healing between all layers (8). A similar problem was encountered for self-healing transistors, which saw a decreased drain current by almost one order of magnitude, owing to im-

perfect alignment of the source and drain electrodes (12).

Self-healing devices have required manual alignment after damage to properly align different functional components, which is impractical for thin devices (<100 μm) (10). When the fractured surfaces of a multilayered device are brought back into contact, even slightly misaligned layers can limit functional recovery. This issue stems from the use of only a single type of self-healing polymer throughout the device. Although using the same polymer for all functional components ensures strong interlayer adhesion, there is no selectivity during healing between different functional components to drive realignment.

We demonstrate a multilayered self-healing device composed of a pair of self-healing polymers with identical dynamic bonds but immiscible polymer backbones. When misaligned after damage, these multilayer structures have composition gradients that drive directional chain diffusion to enable autonomous realignment. Moreover, the similar dynamic bonds between the polymers enable strong interfacial adhesion between the otherwise immiscible layers. We prepared conductive and insulating composites to form thin-film pressure sensors, magnetically assembled soft robots, and underwater circuits, which readily self-heal after mechanical damage. The minimal interlayer diffusion between the polymers also prevents diffusion of the embedded particles, which preserves each layer's electronic function and prevents damage-induced mixing.

Molecular design of immiscible dynamic polymers

We selected polydimethylsiloxane (PDMS) and polypropylene glycol (PPG) as model immiscible backbone polymers because they are flexible,

amorphous polymers with low glass transition temperatures ($T_{g,PDMS} = -125^\circ\text{C}$ and $T_{g,PPG} = -75^\circ\text{C}$) and different bulk surface free energies ($\gamma_{PDMS} \approx 21 \text{ mJ/m}^2$ and $\gamma_{PPG} \approx 31 \text{ mJ/m}^2$) (13, 14). To minimize the effect of film microstructure on self-healing properties, we incorporated a combination of bisurea bonds formed from both 4,4'-methylene bis(phenyl isocyanate) (MPU) and isophorone diisocyanate (IU) into each polymer, which has been shown to produce amorphous, self-healing films without nanoscale aggregation (1, 15–17). The strong directional binding of the MPU units incorporate elasticity into the network, while the weaker binding interactions of the IU units provide a stress-dissipation mechanism to improve bulk toughness and prevent formation of microstructures. For both synthesized polymers, we tuned the MPU:IU ratio and the average backbone molecular weight (M_b) to achieve healing dynamics between 30° and 100°C with solid-like properties at room temperature, which are necessary for device fabrication and stability. The PDMS-based polymer, hereafter referred to as PDMS-HB, has an average M_b of 5 kDa for the PDMS backbone repeat units, an MPU:IU molar ratio of 0.3:0.7, and an overall number-averaged molecular weight (M_n) of 46 kDa [dispersity (D) ~ 1.5]. The PPG-based polymer, hereafter referred to as PPG-HB, has an average M_b of 0.75 kDa for the PPG backbone repeat units, an MPU:IU ratio of 0.5:0.5, and an M_n of 10 kDa ($D \sim 1.7$) (Fig. 1, A and B, and table S1).

We confirmed the lack of larger microstructures by small-angle x-ray scattering (SAXS), which gave characteristic domain spacings of between 6 and 9 nm (Fig. 1C and table S1). Moreover, both polymers exhibit a crossover between the storage and loss modulus between 75° and 85°C (Fig. 1D and table S1) and glass transition temperatures well below room temperature ($T_{g,PDMS-HB} < -80^\circ\text{C}$, $T_{g,PPG-HB} = -35^\circ\text{C}$; fig. S1), which enables experimentally accessible healing dynamics. PPG-HB has less than one-fifth the M_b of PDMS-HB but similar mechanical and thermal properties, which is consistent with previous work that has found that polyethers destabilize hydrogen bond formation and require higher density to achieve a given mechanical property (2). The difference in surface energies between PDMS-HB (23 mJ/m²) and PPG-HB (44 mJ/m²) was experimentally confirmed by contact angle measurements (fig. S2 and tables S1 and S2) (18).

We characterized the self-healing behavior of PDMS-HB and PPG-HB by adapting a recently reported technique, wherein disks of polymer are healed on a parallel plate rheometer with a contact area defined by a polytetrafluoroethylene (PTFE) sheet with a hole (Fig. 1E) (2, 19). After annealing, the plates were pulled apart at a constant rate to generate stress-displacement curves, similar to those obtained



¹Department of Chemical Engineering, Stanford University, Stanford, CA 94305, USA. ²Department of Mechanical Engineering, Stanford University, Stanford, CA 94305, USA.

*Corresponding author. Email: zbao@stanford.edu

†These authors contributed equally to this work.

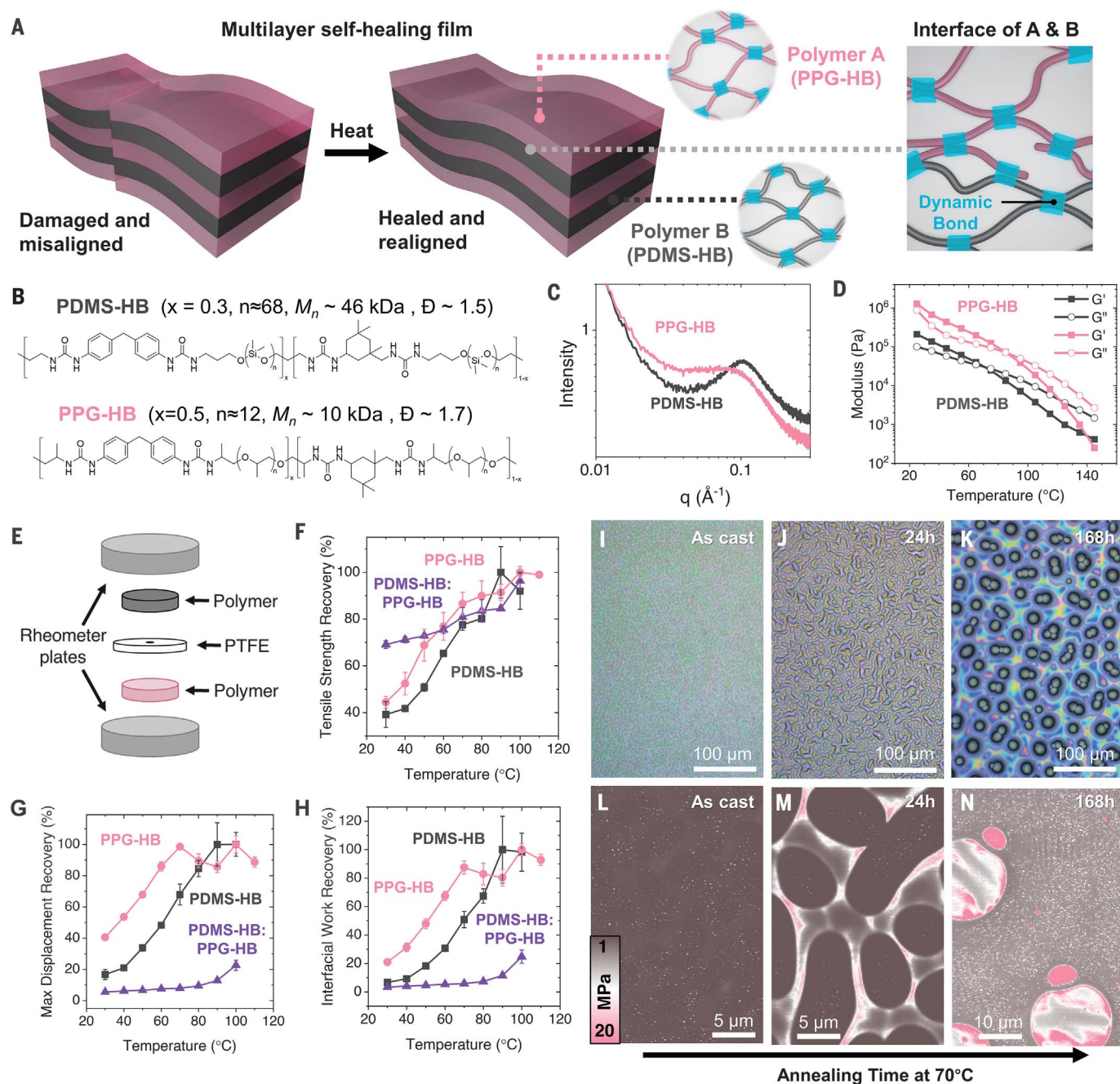


Fig. 1. Design and characterization of a pair of dynamic polymers—PDMS-HB and PPG-HB—with immiscible backbones and identical hydrogen bonding units. (A) Schematic showing the principle of surface tension-mediated realignment and healing of a fractured multilayer laminate.

The difference in surface energy between the two polymer backbones (type A and type B) drives realignment, while the dynamic bonds in both polymers promote interlayer adhesion for device performance. (B) Chemical structures of the two immiscible dynamic polymers used in this study, PDMS-HB and PPG-HB. x , mole fraction of MPU; n , average number of monomers in the backbone segment between dynamic bonds. (C) SAXS curves showing the amorphous structure of PDMS-HB (black) and PPG-HB (pink) with domain sizes of ~ 6 to 9 nm. (D) Rheological characteristics of PDMS-HB (black) and PPG-HB (pink) showing the crossover between the storage modulus (G' , solid squares) and

loss modulus (G'' , open circles) around 75° to 85°C . This crossover point corresponds to the onset of flow in the bulk materials. (E) Schematic of the experimental setup of the self- or interfacial healing between two polymers. The recovery in tensile strength (F), max displacement (G), and interfacial work (H) for self-healed PDMS-HB (black squares), self-healed PPG-HB (pink circles), and PDMS-HB healed with PPG-HB (purple triangles). Each point is averaged over three samples, with a healing time of 30 min at the specified temperature. Optical microscope images of a spin-coated film of PDMS-HB and PPG-HB (50 wt %) immediately after casting (I) and after annealing at 70°C for 24 hours (J) and 168 hours (K), and the corresponding AFM nanomechanical images (L to N). Phase separation increases with increased annealing time. The modulus of neat PDMS-HB and PPG-HB measured by AFM are 1 and 20 MPa, respectively, suggesting that the pink regions are PPG-rich.

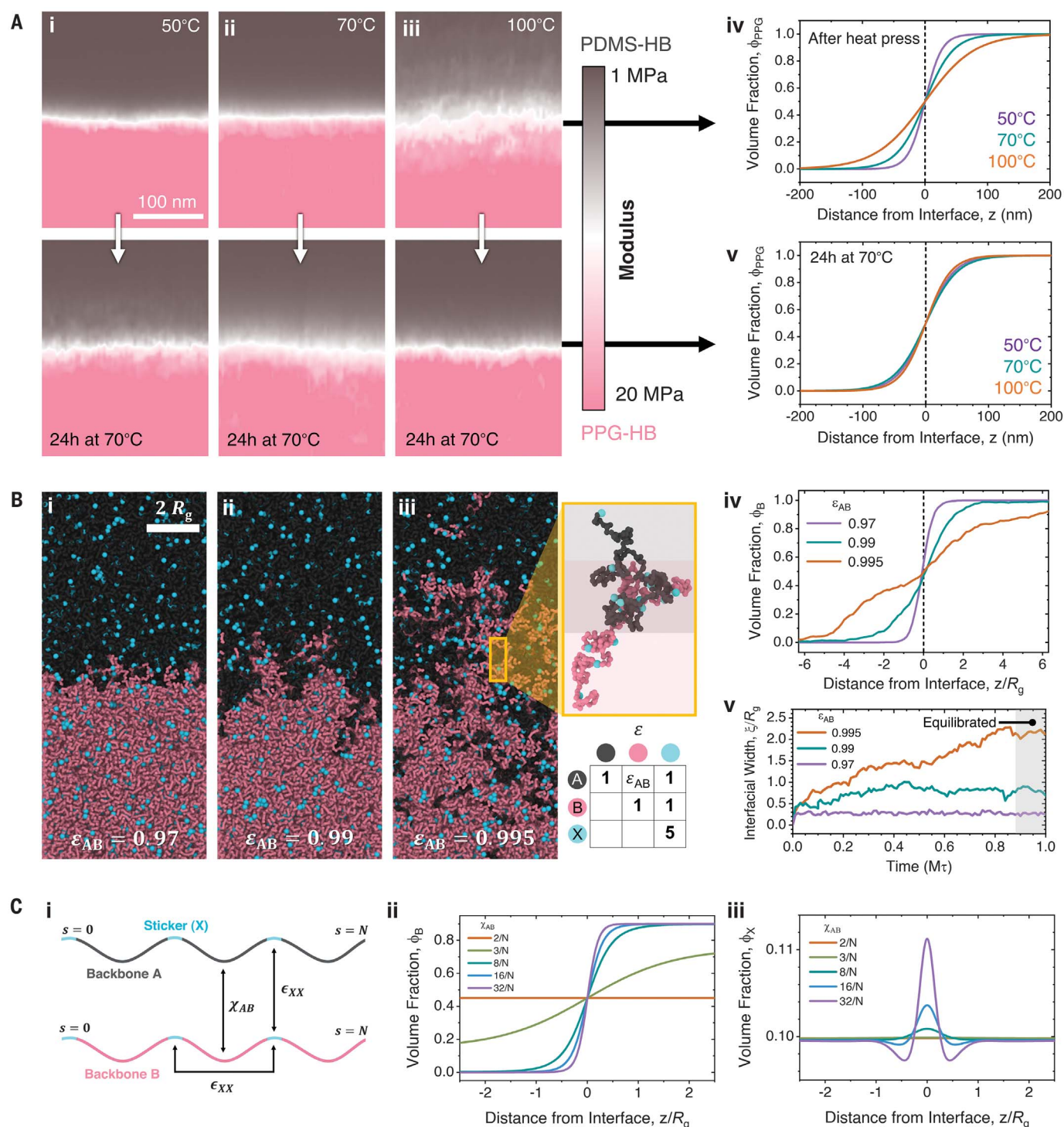


Fig. 2. The interface between two immiscible dynamic polymer networks with identical dynamic bonds.

(A) AFM characterization of the modulus gradient across the interfaces of bilayer films prepared by gently hot pressing (~ 20 kPa) at (i) 50°C, (ii) 70°C, and (iii) 100°C, before (top) and after (bottom) annealing for 24 hours at 70°C. The higher-modulus region corresponds to pure PPG-HB (pink), and the lower-modulus region corresponds to pure PDMS-HB (dark gray). Fitted interfacial profiles obtained from the AFM images (iv) immediately after hot pressing and (v) after annealing for 24 hours at 70°C, showing that the interfaces are at thermodynamic equilibrium. **(B)** Coarse-grained molecular dynamics simulation snapshots for equilibrated interfaces with (i) $\epsilon_{AB} = 0.97$, (ii) $\epsilon_{AB} = 0.99$, and (iii) $\epsilon_{AB} = 0.995$. Inset shows chains at the interface with two different polymer

backbones (A beads, black; B beads, pink) and identical dynamic bonds (X beads, blue). Table gives the relative energetic attraction between different bead types. (iv) Fitted interfacial profiles obtained from the equilibrated simulations. (v) Dynamics of the fitted interfacial width during simulation while approaching equilibrium. **(C)** (i) Schematic of the field-theoretic model, showing two polymer backbones (A, gray; B, pink) with a repulsive χ_{AB} interaction, an identical dynamic bond (X, blue) with an attractive ϵ_{XX} interaction, and a chain length of N . (ii) Interfacial profiles predicted by the field-theoretic model for different values of χ_{AB} normalized by chain length: 2/ N (orange), 3/ N (green), 8/ N (teal), 16/ N (blue), and 32/ N (purple). (iii) Sticker volume fraction across the interface for the same χ_{AB} values, showing that dynamic bonds cluster at the interface with increasing χ_{AB} .

on an extensometer (figs. S3 and S4). We repeated this process for different temperatures in 10°C steps and monitored healing by tracking the recovery in the tensile strength (Fig. 1F), the max displacement (Fig. 1G), and the interfacial work (i.e., the area under the stress-displacement curve; Fig. 1H) as a function of healing temperature (fig. S3). In all cases, we observed a plateau at higher temperatures indicative of full healing. Both PDMS-HB and PPG-HB were fully healed after 30 min at ~80° to 90°C, consistent with their terminal flow onset temperatures (Fig. 1D and table S1). These results are also consistent with experimental work on interfacial healing of metallosupramolecular polymers as well as theoretical and computational predictions (20–22).

We next evaluated the interfacial healing between PDMS-HB and PPG-HB, which have identical dynamic bonds but immiscible polymer backbones. The self-healing of two polymeric interfaces involves wetting between the two-dimensional (2D) interfaces and then creation of a 3D interphase that propagates with macromolecular diffusion and possibly polymer reentanglement to restore bulk properties (23). Neumann *et al.* found that for self-healing of metallosupramolecular polymers, full healing was achieved only when the 3D interphase reached widths on the order of ~100 nm (20). We hypothesized that the use of similar dynamic bonds would enable wetting and adhesion of the 2D interface, while the difference in surface free energies between PDMS-HB and PPG-HB would limit the width of a 3D interphase, approaching the limiting case of two fully immiscible polymer blends (24, 25). Compared with the self-healing cases, the PDMS-HB:PPG-HB interface exhibited reduced healing, even at 100°C, when both samples exhibit rapid dynamics and liquid-like behavior. The tensile strength recovered almost immediately to ~70% of the PDMS-HB pristine interface, indicative of good wetting between the surfaces. However, both the max displacement and interfacial work recoveries remained lower (<20%) than the healed samples with two pieces of identical polymers (Fig. 1, F to H).

These results suggest that healing between the samples is thermodynamically restricted because of a lack of macromolecular diffusion across the interface. To further test this hypothesis, we spin-coated a film of PDMS-HB and PPG-HB (50 wt % blend) from a homogeneous solution and then annealed the sample at 70°C for various lengths of time. Optical microscope images (Fig. 1, I to K) and atomic force microscopy (AFM) images (Fig. 1, L to N) showed increasing phase separation with increased annealing, with coarsening occurring across all measured length scales. These observations suggest that PDMS-HB and PPG-HB are thermodynamically immiscible and explain

the limited healing observed between the two polymers. In addition, we measured interfacial healing between PDMS-HB and PPG-HB at 70°C for longer healing times and showed that minimal additional healing occurred (fig. S5). This finding implies that increased healing at higher temperatures (Fig. 1, F to H) arises not from faster polymer dynamics but rather from increased miscibility.

Interface between two immiscible dynamic polymers

To further test this hypothesis, we characterized the interface between PDMS-HB and PPG-HB through a combination of experiments, simulation, and theory. We laminated two layers of PDMS-HB and PPG-HB together by gently hot pressing (~20 kPa of pressure; fig. S6) at different temperatures and then measured cut interfaces by AFM before and after annealing at 70°C (26, 27). Tracking changes in the modulus revealed an interface between PDMS-HB and PPG-HB (Fig. 2A), whose width we measured quantitatively by fitting to a sigmoidal function (Eq. 1), analogous to the analytic solution by Helfand and Tagami for the interface between two immiscible polymers (24)

$$\phi(z) = \frac{1}{1 + e^{-(z-z_0)/\xi}} \quad (1)$$

$\phi(z)$ is the volume fraction of one polymer as a function of position, z_0 is the location of the interface, and ξ is a measure of the interfacial width. The fitted interfacial widths (ξ) increased with increasing hot-pressing temperature with values of 13 ± 1 , 23 ± 1 , and 39 ± 1 nm for 50°, 70°, and 100°C hot-pressed films, respectively (Fig. 2A and fig. S7). However, if subsequently annealed at the same temperature, all films exhibited similar interfacial widths (Fig. 2A and fig. S7) of 23 ± 1 , 26 ± 2 , and 20 ± 1 nm for the initially 50°, 70°, and 100°C hot-pressed films, respectively. These observations suggest that the interfaces are at thermodynamic equilibrium during hot pressing and annealing. Moreover, these interfaces were all measured at room temperature, without rapid quenching, which means that the interfacial width (and thus the interlayer adhesion) can be programmed at a specific temperature and then locked in place by cooling the chains into a kinetically trapped state. To demonstrate this concept, we performed an interfacial healing experiment at 100°C for 30 min with an additional annealing step at 70°C for 30 min (fig. S8). Consistent with the decreased interfacial width measured after annealing, the interfacial work between the two polymers decreased with the additional annealing step.

We also estimated the interdiffusion depth of PDMS-HB into bulk PPG-HB by performing x-ray photoelectron spectroscopy (XPS) on interfaces healed for 30 min at 70° and 100°C and

then mechanically separated at room temperature. We saw a clear decrease in the Si/C ratio with increased sputtering, which allowed us to estimate the molar fraction of PDMS-HB as a function of depth from the interface (figs. S9 and S10). This yielded an interfacial width (ξ) of 7 nm at 100°C and 2 nm at 70°C. The increased interfacial width at higher temperature matches the trend observed through AFM.

We next sought to model this process in a general manner by conducting coarse-grained molecular dynamics simulations of the interface between two identical polymers containing identical dynamic bonds but immiscible backbones (Fig. 2B) (28, 29). We periodically spaced dynamic bonding beads along the polymer backbone with increased interaction energy ($\epsilon_R = 5\epsilon$) relative to the backbone beads ($\epsilon_P = 1\epsilon$). Following previous simulations of homopolymers, immiscibility of the backbones was introduced by decreasing the interaction energy between distinct backbone beads from $\epsilon_{AB} = 1\epsilon$ (self-healing) to $\epsilon_{AB} = 0.95\epsilon$ (entirely immiscible) (30). Independently prepared slabs of the two polymer species were brought together in the melt state and allowed to interdiffuse over time until the interface reached a thermodynamic equilibrium (Fig. 2B). Throughout the simulation, the interfacial width was tracked as a function of time by fitting Eq. 1 to the extracted density profiles (Fig. 2B). Consistent with experiments, we observed a sigmoidal density profile and that the equilibrium interfacial width (measured as a correlation length by fitting to Eq. 1) decreased with increasing backbone immiscibility.

Finally, we developed a field-theoretic description of the interface between two immiscible polymer backbones (denoted by A or B monomers) with the same dynamic bonding units (denoted by X monomers). The model predicts the monomer density profiles for an incompressible melt of AX and BX block copolymers of the same chain length N , whose interactions are dominated by a pairwise, repulsive χ parameter between A and B monomers (χ_{AB}) and a pairwise, attractive parameter between X monomers (ϵ_{XX}) (Fig. 2C). With increasing χ_{AB} , analogous to decreasing temperature in experiments, we observed a decrease in the interfacial width between the polymers (Fig. 2C). In addition, we also observed an increase in sticker clustering at the AX-BX interface with increasing χ_{AB} (Fig. 2C), where stickers at the interface reduced the system free energy by minimizing the number of A-B contacts. This is further supported by the fact that the density profiles are almost independent of ϵ_{XX} (fig. S11).

The combination of experiments, simulation, and theory suggest that with increasing temperature, the interface between two immiscible dynamic polymers is governed by a decreasing

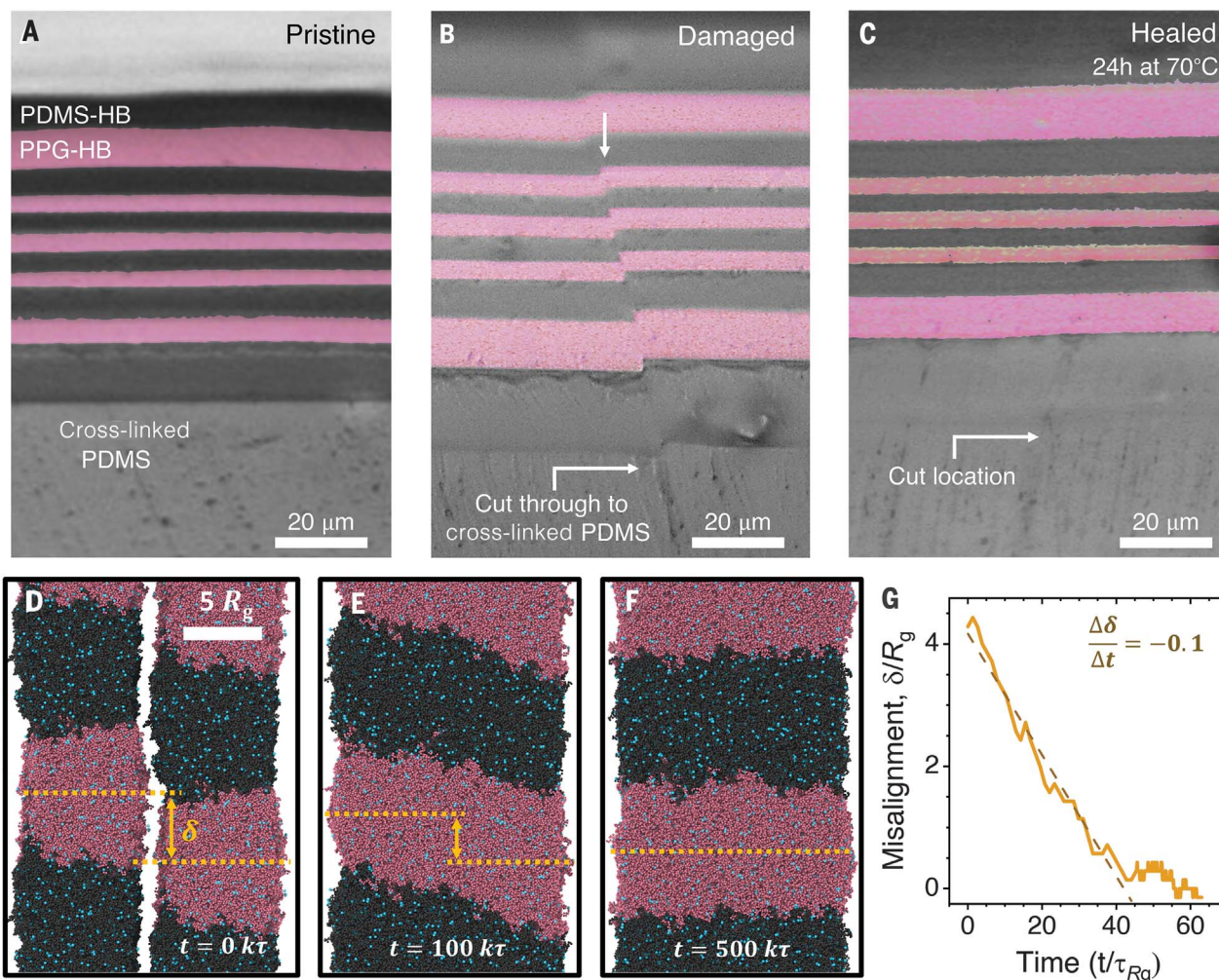


Fig. 3. Autonomous alignment and healing between immiscible dynamic polymers in a multilayered film. Cross-sectional optical microscope images of (A) the pristine hot-pressed multilayer laminate, (B) the damaged and misaligned laminate, and (C) the healed and realigned laminate after annealing for 24 hours at 70°C. A small amount of blue dye was added to PPG-HB for optical contrast, which appears pink in dark-field images at higher magnifications. The cross-linked

PDMS substrate (bottom layer) was unable to heal and marks the damage site.

(D to F) Simulation snapshots showing how an initially misaligned and separated laminate aligns and heals over time. (G) Misalignment distance (δ), normalized by the chain R_g , decreases linearly with simulation time, normalized by the time to diffuse one chain R_g (τ_{R_g}), until alignment is achieved. The slope of -0.1 corresponds to a realignment rate of $0.1R_g$ per τ_{R_g} .

χ parameter (χ_{AB}) between the polymer backbones, which increases the interfacial width. In addition, dynamic bonds cluster at the interface to reduce contacts between the immiscible backbones. When normalized by estimated radius of gyration, R_g , values for PDMS-HB and PPG-HB (~ 6 and ~ 3 nm, respectively, assuming homopolymers with similar M_n), the interfacial widths measured experimentally by AFM are larger than those observed in simulations or predicted by theory (31). However, the normalized interfacial widths obtained by XPS are well within the observed values. We attribute the larger interfacial widths measured by AFM to finite tip-size broadening during the indentation measurement but note that the important qualitative trends remain consistent across experiments, simulation, and theory (32). More-

over, the consistency between experiments, simulation, and theory suggests that these models could be used to screen polymer backbones and dynamic bonding linkers for desirable mechanical and healing properties.

Autonomous alignment and healing of multilayered polymer films

We next tested the healing of multilayer films of PDMS-HB and PPG-HB. We hypothesized that the reduced interfacial healing between the polymers would enable autonomous realignment of the films after damage. Taking advantage of the immiscibility of PDMS-HB and PPG-HB, we stacked alternating films with a thickness of ~ 100 μm and hot pressed them to a final film with a thickness of ~ 70 μm and 11 alternating layers, with individual thick-

nesses ranging from 3 to 15 μm (Fig. 3A). The resulting film was placed on a cross-linked PDMS substrate and then cut in half. Figure 3B shows the misalignment between the alternating layers as well as the cut extending into the cross-linked PDMS substrate. During healing, the layers autonomously realigned and reformed sharp and alternating interfaces between the PDMS-HB and PPG-HB (Fig. 3C). The misaligned cut in the cross-linked PDMS (which was not able to self-heal) remains visible. When the same type of dynamic polymer was used for both layers, autonomous realignment during healing was not observed (fig. S12).

The phenomenon of autonomous realignment and healing in multilayer structures was also observed in our coarse-grained simulation model. In the simulation, polymer surfaces

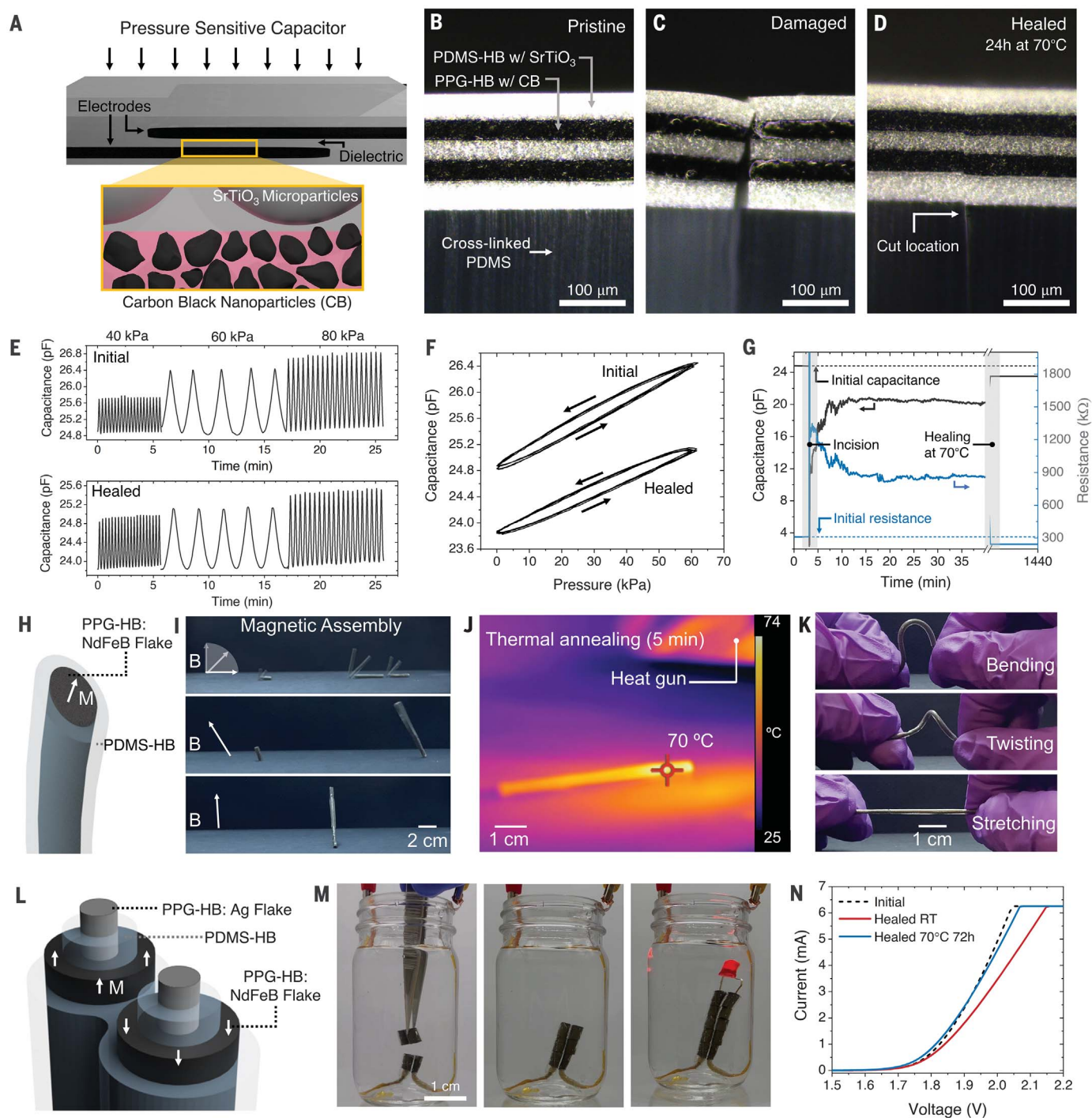


Fig. 4. Demonstration of functional layer recognition and healing in soft electronic devices based on dynamic polymer composites. (A) Schematic of a pressure sensitive capacitor with electrodes made from a PPG-HB:carbon black 4:1 weight ratio composite, and dielectric layers made from a PDMS-HB: SrTiO₃ 4:1 weight ratio composite. Dark-field optical images of the cross sections of the initial capacitor (B), the capacitor after fracture showing layer misalignment (C), and the healed device after realignment during annealing for 24 hours at 70°C (D). (E) Initial (top) and healed (bottom) pressure-sensing performance as a time series. Capacitance was monitored while cyclically applying pressures ranging from 0 to 80 kPa. (F) Capacitance versus pressure showing the linear dependence of the capacitance on pressure, with minimal change in drift and hysteresis between the initial (top) and healed (bottom)

sensor. (G) Series capacitance and resistance as the device is cut and healed at room temperature, and after annealing at 70°C. (H) Schematic of core-shell magnetic fibers made from a PPG-HB:NdFeB flake 1:4 weight ratio composite and PDMS-HB. (I) Magnetic assembly of the core-shell fibers. (J) Thermal welding of the assembled fiber at 70°C for 5 min with a heat gun. (K) Images of the welded device bending, twisting, and stretching to show mechanical robustness. (L) Schematic of double core-shell fibers with separate electrically conductive (PPG-HB:Ag flake 1:1 weight ratio composite) and magnetic (PPG-HB:NdFeB flake 1:4 weight ratio composite) layers with PDMS-HB shells. (M) Images of the underwater circuit assembly of the LED. (N) Current–voltage sweeps of the initial device (dashed black), after room temperature underwater healing (solid red), and after annealing at 70°C for 72 hours (solid blue).

fused together with an initial misalignment (denoted δ) and then selectively interdiffused and steadily realigned until reaching complete alignment (Fig. 3, D to G, and fig. S13). The correspondence between simulation and experiment suggests that this phenomenon can be generalized to other pairs of polymers to simultaneously achieve strong interlayer adhesion and selective interlayer healing.

Demonstration of functional healing for soft electronics

To demonstrate that the use of alternating layers of immiscible dynamic polymers could promote alignment during the healing of a thin (~10 to 100 μm) multilayered electronic device, we investigated the functional healing of a pressure-sensitive capacitor (Fig. 4A). The capacitor was made from alternating layers of homogeneous composites of PDMS-HB embedded with dielectric strontium titanate (SrTiO_3) microparticles (20 wt %) and PPG-HB embedded with conductive carbon black nanoparticles (20 wt %). Figure 4, B to D, shows microscope images of a cross section of the parallel plate capacitor in the pristine, damaged, and healed states. Even when misaligned after damage, the multilayer capacitor realigned during healing and recovered its sensing capability, exhibiting quantitatively similar pressure-sensing performance when subjected to the same cyclic loading conditions (Fig. 4, E and F). We also monitored the change in the series capacitance and resistance immediately after damage (Fig. 4G). Only a partial recovery of the capacitance was observed at room temperature, and microscope images of the edge of the device showed misaligned layers (Fig. 4C). However, after heating, the layers almost completely realigned (Fig. 4D), and the device recovered 96% of its initial capacitance. Mechanical recovery was also confirmed by manually applying a tensile force to the sample, resulting in fracture of the underlying substrate while maintaining integrity of the healed layers (fig. S14).

As an additional demonstration of the utility of this pair of selectively weldable dynamic polymers, we fabricated core-shell fiber structures with composites containing magnetic NdFeB microflakes (~10 μm , 80 wt %) embedded in PPG-HB as the core material and PDMS-HB as the shell material (Fig. 4H). These fibers are magnetized along their longitudinal directions with an impulse magnetizer (1.5 T). When cut into pieces, the fibers' motion could be controlled with an external magnetic field to achieve rigid body rotations for reassembling without any manual alignment. When close in distance, these fibers exhibited a magnetic attractive force that induced a contact pressure to promote selective welding of the layers (Fig. 4I and movie S1). After thermal welding at 70°C, the magnetically assembled

fibers could withstand bending, twisting, and stretching deformations (Fig. 4, J and K). In contrast to single-component magnetic self-healing, which achieves macroscopic assembly of pieces but lacks the precision for microscopic alignment, this work shows that we can simultaneously employ two alignment mechanisms: magnetically guided macroscopic alignment and interfacial-tension mediated microscopic alignment (33–36).

Building on this demonstration, we fabricated multilayered magnetic wires with a conductive core, an insulating shell, a magnetized layer, and an outer encapsulating shell (Fig. 4L). Two wires with opposite magnetic orientation were assembled to make a light-emitting diode (LED) circuit. Upon cutting the wires into four pieces, the circuit could be reassembled by adding the components into a glass vial filled with water, where the magnetic forces guided the assembly of the wire to achieve almost instantaneous electrical healing, illuminating an LED (Fig. 4M, fig. S15, and movie S2). The magnetic forces guided the alignment of the two terminals of the LED in the correct orientation with respect to the voltage source (+3 V) and ground. Comparison of current-voltage sweeps showed comparable turn-on voltages before and after healing (Fig. 4N), with full mechanical and electrical healing achieved after thermal annealing at 70°C for 72 hours.

In this study, we achieved autonomous alignment during the self-healing of multilayered soft electronic devices by using two immiscible dynamic polymers, whose different backbones enabled interfacial tension-mediated realignment after damage. We used the same dynamic bond in both polymers to maintain strong interlayer adhesion required for a stretchable device. The interfacial width between the polymers, which subsequently determines the interlayer adhesion, can be programmed by annealing temperature. Simulation and theory results suggest that this design concept can be readily extended to other molecular systems. We fabricated thin-film healable pressure sensors, magnetically assembled and welded structures, and self-healable underwater circuits that autonomously realign during healing to demonstrate the capabilities of this approach.

REFERENCES AND NOTES

- J. Kang et al., *Adv. Mater.* **30**, e1706846 (2018).
- Y. Yanagisawa, Y. Nan, K. Okuro, T. Aida, *Science* **359**, 72–76 (2018).
- P. Cordier, F. Tournilhac, C. Soulié-Ziakovic, L. Leibler, *Nature* **451**, 977–980 (2008).
- C.-H. Li et al., *Nat. Chem.* **8**, 618–624 (2016).
- Y.-L. Rao et al., *J. Am. Chem. Soc.* **138**, 6020–6027 (2016).
- S. C. Grindy et al., *Nat. Mater.* **14**, 1210–1216 (2015).
- R. J. Wojtecki, M. A. Meador, S. J. Rowan, *Nat. Mater.* **10**, 14–27 (2011).
- D. Son et al., *Nat. Nanotechnol.* **13**, 1057–1065 (2018).
- M. Khatib, O. Zohar, W. Saliba, H. Haick, *Adv. Mater.* **32**, e2000246 (2020).
- M. Khatib, O. Zohar, H. Haick, *Adv. Mater.* **33**, e2004190 (2021).
- Y. J. Tan et al., *Nat. Mater.* **19**, 182–188 (2020).

- M. Khatib et al., *Small* **15**, e1803939 (2019).
- G. Wypych, in *Handbook of Polymers* (ChemTec Publishing, ed. 2, 2016), pp. 340–344.
- G. Wypych, in *Handbook of Polymers* (ChemTec Publishing, ed. 2, 2016), pp. 517–519.
- D. Döhler et al., *ACS Appl. Polym. Mater.* **2**, 4127–4139 (2020).
- C. B. Cooper et al., *J. Am. Chem. Soc.* **142**, 16814–16824 (2020).
- C. B. Cooper et al., *ACS Cent. Sci.* **7**, 1657–1667 (2021).
- A. Faghinijad et al., *Adv. Funct. Mater.* **24**, 2322–2333 (2014).
- Y. Fujisawa, A. Asano, Y. Itoh, T. Aida, *J. Am. Chem. Soc.* **143**, 15279–15285 (2021).
- L. N. Neumann et al., *Sci. Adv.* **7**, eabe4154 (2021).
- E. B. Stukalin, L.-H. Cai, N. A. Kumar, L. Leibler, M. Rubinstein, *Macromolecules* **46**, 7525–7541 (2013).
- Z. Shen, H. Ye, Q. Wang, M. Kröger, Y. Li, *Macromolecules* **54**, 5053–5064 (2021).
- R. P. Wool, K. M. O'Connor, *J. Appl. Phys.* **52**, 5953–5963 (1981).
- E. Helfand, Y. Tagami, *J. Polym. Sci. B* **9**, 741–746 (1971).
- G. H. Fredrickson, *The Equilibrium Theory of Inhomogeneous Polymers*, vol. 134 of International Series of Monographs on Physics (Oxford Univ. Press, 2006).
- C. He, S. Shi, X. Wu, T. P. Russell, D. Wang, *J. Am. Chem. Soc.* **140**, 6793–6796 (2018).
- K. Hu et al., *Macromolecules* **52**, 9759–9765 (2019).
- A. Stukowski, *Model. Simul. Mater. Sci. Eng.* **18**, 015012 (2009).
- A. P. Thompson et al., *Comput. Phys. Commun.* **271**, 108171 (2022).
- T. Ge, G. S. Grest, M. O. Robbins, *ACS Macro Lett.* **2**, 882–886 (2013).
- L. J. Fetters, D. J. Lohse, D. Richter, T. A. Witten, A. Zirkel, *Macromolecules* **27**, 4639–4647 (1994).
- Q. D. Nguyen, K.-H. Chung, *Ultramicroscopy* **202**, 1–9 (2019).
- A. J. Bandothkar et al., *Sci. Adv.* **2**, e1601465 (2016).
- X. Kuang et al., *Adv. Mater.* **33**, e2102113 (2021).
- S. Wu et al., *ACS Appl. Mater. Interfaces* **11**, 41649–41658 (2019).
- Q. Ze et al., *Adv. Mater.* **32**, e1906657 (2020).

ACKNOWLEDGMENTS

Funding: This work was supported by Army Research Office Materials Design Program, grant W911NF-21-1-0092 (Z.B.); National Science Foundation Career Award CMMI-2145601 (R.Z.); National Science Foundation Award CMMI-2142789 (R.Z.); Department of Defense, National Defense Science & Engineering Graduate Fellowship Program (C.B.C.); Walter Benjamin Fellowship Program, Deutsche Forschungsgemeinschaft DFG 456522816 (L.M.); and TomKat Center Fellowship for Translational Research at Stanford University (S.T.O.). Part of this work was performed at the Stanford Nano Shared Facilities (SNSF), supported by the National Science Foundation under award ECCS-1542152. Use of the Stanford Synchrotron Radiation Lightsource, SLAC National Accelerator Laboratory, for SAXS experiments was supported by the US Department of Energy, Office of Science, Office of Basic Energy Sciences, under contract DE-AC02-76SF00515. This work used Expanse computing resources at the San Diego Supercomputer Center through allocation MAT220035 from the Advanced Cyberinfrastructure Coordination Ecosystem: Services & Support (ACCESS) program, which is supported by National Science Foundation grants 2138259, 2138286, 2138307, 2137603, and 2138296. **Author contributions:** Conceptualization: C.B.C., S.E.R., and Z.B. Methodology: C.B.C., S.E.R., L.M., and J.Q. Investigation: C.B.C., S.E.R., L.M., S.W., J.-C.L., M.K., and S.T.O. Visualization: C.B.C., S.E.R., and Z.B. Writing – original draft: C.B.C., S.E.R., and Z.B. Writing – review & editing: C.B.C., S.E.R., L.M., S.W., J.-C.L., M.K., S.T.O., R.Z., J.Q., and Z.B. Supervision: Z.B., J.Q., and R.Z. **Competing interests:** A US provisional patent on this work (serial number 63/440,656) was filed on 23 January 2023 by Z.B., C.B.C., and S.E.R. The authors declare that they have no other competing interests. **Data and materials availability:** All data are available in the main text or the supplementary materials. **License information:** Copyright © 2023 the authors, some rights reserved; exclusive licensee American Association for the Advancement of Science. No claim to original US government works. <https://www.science.org/about/science-licenses-journal-article-reuse>

SUPPLEMENTARY MATERIALS

science.org/doi/10.1126/science.adh0619
Materials and Methods
Supplementary Text
Figs. S1 to S15
Tables S1 and S2
References
Movies S1 and S2

Submitted 14 February 2023; accepted 14 April 2023
10.1126/science.adh0619



Autonomous alignment and healing in multilayer soft electronics using immiscible dynamic polymers

Christopher B. Cooper, Samuel E. Root, Lukas Michalek, Shuai Wu, Jian-Cheng Lai, Muhammad Khatib, Solomon T. Oyakhire, Renee Zhao, Jian Qin, and Zhenan Bao

Science, **380** (6648), .

DOI: 10.1126/science.adh0619

Editor's summary

One advantage of using soft materials for robotic devices is that there is greater scope for self-healing, but a challenge for multilayer devices is to ensure realignment after damage. Cooper *et al.* present a method for healing multilayered and functional polymer materials by showing how a combination of dynamic hydrogen-bonding interactions and phase separation between different polymeric building blocks can be leveraged to achieve simultaneous autonomous realignment and healing of multilayered polymer films. This approach can restore both the mechanical and functional properties of complex polymer composites and even enables underwater self-assembly. —Marc S. Lavine

View the article online

<https://www.science.org/doi/10.1126/science.adh0619>

Permissions

<https://www.science.org/help/reprints-and-permissions>

Use of this article is subject to the [Terms of service](#)

Science (ISSN) is published by the American Association for the Advancement of Science. 1200 New York Avenue NW, Washington, DC 20005. The title *Science* is a registered trademark of AAAS.

Copyright © 2023 The Authors, some rights reserved; exclusive licensee American Association for the Advancement of Science. No claim to original U.S. Government Works